JOURNAL OF THERMOPHYSICS AND HEAT TRANSFER
Vol. 11, No. 3, July–September 1997

Turbulent Heat Transfer and Fluid Flow in a Porous-Baffled Channel

Jenn-Jiang Hwang*
Chung-Hua Polytechnic Institute, Hsinchu 30067, Taiwan, Republic of China

Experiments were conducted to examine the effect of porous-type baffles on heat transfer and friction in a baffled channel. The porous-type baffles are arranged on the bottom and top channel walls in a staggered manner. Flowfield, pressure loss, isotherm pattern, and channel centerline heat transfer coefficients are obtained inside the periodic cell formed between the segmented baffles. Results of the conventional solid-type-baffled channel are also obtained for comparison. The void fraction v_0 of porous-type baffle and the baffle spacing S/H are fixed at 0.42, and 1.0, respectively; whereas the baffle height ratio h/H varies from 0.25 to 0.75 and the flow Reynolds number Re ranges from 1×10^4 to 5×10^4, respectively. It is disclosed that the flow patterns around the porous- and solid-type baffles are entirely different. These different transport phenomena, in conjunction with the change in baffle effectiveness significantly influence the local heat transfer coefficient distributions but negligibly influence the average heat transfer coefficients. Relative to the solid-type-baffled channel, the porous-type-baffled channel has a lower friction loss. Consequently, the porous-type-baffled channel yields a better thermal performance under constant pumping power. Compact correlations for the average Nusselt number and friction factor are also developed in terms of flow and baffled parameters.

Nomenclature

A = surface area of the smooth channel
De = channel hydraulic diameter, $2WH/(W + H)$
f = friction factor for the baffled channel
f_s = friction factor for the smooth channel
G = mass flux
H = channel height, Fig. 2
h = baffle height, Fig. 2
K = loss coefficient, $2\Delta P/(\rho U_b^2)$
k_e = effective thermal conductivity of the baffle
k_f = air thermal conductivity
Nu = local Nusselt number
$\overline{Nu}$ = average Nusselt number for periodically fully developed baffled channel flow
$\overline{Nu}_s$ = average Nusselt number for the smooth channel, at the same mass flow rate
$\overline{Nu}_s^*$ = average Nusselt number for the smooth channel, at the same pumping power
P = pressure
Pr = Prandtl number
Q = electrical power supplied by thermofoil
$Q_{\rm ac}$ = axial convective heat loss from the ends of the test section
$Q_{\rm bc}$ = convective heat loss from the back side of the heated wall
$Q_{\rm conv}$ = convective heat transfer from the channel wall into the coolant
$Q_{\rm loss}$ = heat loss
Q_r = radiative heat loss from the test section to ambient
Re = Reynolds number, $U \cdot De/\nu$
Re^* = $(f/f_s)^{1/3} \cdot Re$
S = baffle spacing, Fig. 2
T = local air temperature
T_{b0} = bulk mean temperature of air at channel outlet
$\bar{T}_b$ = bulk mean temperature of air
$T_{\rm in}$ = air temperature at channel inlet, i.e., room temperature
$\bar{T}_w$ = average wall temperature
t = baffle thickness, Fig. 2
U = streamwise mean velocity of the airflow
U_b = bulk velocity, $\int_0^H U \, dY/H$
u = streamwise fluctuation velocity
V = vertical mean velocity of the airflow
v_0 = void fraction (or porosity) of the baffle, $(\upsilon_t - \upsilon_s)/\upsilon_t$
W = channel width, Fig. 2
X = axial coordinate, Fig. 2
Y = vertical coordinate, Fig. 2
Z = spanwise coordinate, Fig. 2
ΔP = pressure drop across two pressure taps
ΔX = axial distance between two pressure taps
ε = emissivity of the heated plate
ρ_a = air density
ρ_b = density of the baffle
υ_s = total volume of the bronze beads within a porous-type baffle
υ_t = total volume of the baffle

Subscripts

b = bulk mean
s = smooth
w = wall

Introduction

ATTACHING fin–baffles on heat transfer surfaces is an effective means for heat transfer augmentation and is often encountered in many industrial applications. The shell-and-tube heat exchanger is a familiar example. Usually, thermal resistance is larger on the shell side, and the baffles are spread along the tube bundle to guide the fluid to move perpendicularly to the tubes and thus increase its heat transfer rate. In addition, the baffles attached to the walls of the flow passages could provide additional heat transfer surface area and promote turbulence. Comparable transport phenomena also happen in gas-cooled solar collectors, shell-and-plate mixing chambers, some electronic circuit boards, and in limited cases, for the flow through some labyrinth shaft seals. The study of baffle-

---

Received July 15, 1996; revision received Dec. 23, 1996; accepted for publication Dec. 27, 1996.

*Associate Professor, Department of Mechanical Engineering. E-mail: jjhwang@chpi.edu.tw.

walled-channel heat exchangers has recently attracted widespread attention. A large amount of useful information is available in the literature. Many investigations have been conducted toward establishing an optimal baffle geometry that gives the best heat transfer performance for a given pumping power or flow rate. Appropriate geometric parameters discussed in previous works include baffle height (or window cut ratio), baffle spacing, and the relative arrangement of baffles. For the sake of brevity, only some relevant works will be cited. In the experimental efforts, general qualitative measurements of the flowfield in a heat exchanger with segmental baffles originated from Gunter et al.[1] They presented many flow visualization pictures to examine the main features of the flow around the baffles. The works covered a wide range of flow velocity, baffle spacing, and baffle height. However, no quantitative information about the mean flow velocity and turbulence was provided in their work. Gay et al.[2] conducted an experiment to determine the local mass transfer coefficients of the shell-side surfaces by an electrochemical mass transfer technique. A complete literature review was also provided in their work. Founti and Whitelaw[3] utilized laser-Doppler anemometer (LDA) to deduce the velocity field in a modeled axisymmetric heat exchanger with disk–doughnut baffles on the shell-side surfaces. It was found that similar distributions of the mean-flow velocity and turbulent intensity were achieved after two sets of baffles (i.e., four baffles) from the channel entrance for $2.5 \times 10^4 < Re < 4.6 \times 10^4$. Later, LDA was also employed by Berner et al.[4] to measure the mean flow velocity and turbulence intensity distributions inflow around segmental baffles of different heights and spacing. Some flow visualization photographs were also given at low Reynolds numbers. Results of the developed lengths and pressure loss coefficients were presented. Habib et al.[5] experimentally investigated the effects of baffle height and baffle conductivity on the heat transfer and flow characteristics in a rectangular channel. The results indicated that the associated increase of pressure loss was much higher than the increase in heat transfer coefficient as the baffle height is increased. Relevant predictions of the flow and heat transfer in baffled channels included the works of Refs. 6–10.

From the previous discussion of the available literature, it is noted that the segmented baffles employed in all of the previous investigations are solid. Therefore, a systematically experimental study on the heat transfer and fluid flow in a rectangular channel with porous-type baffles, in contrast to the aforementioned solid-type baffles, would be urgent and worthwhile. This motivates the present work that is to experimentally examine the effect of the porous-type baffles on the fluid flow and heat transfer in a rectangular channel. First, experiments are conducted to compare the mean and fluctuating velocity profiles and isothermal contours between flow around the porous- and solid-type baffles, which will provide a very sound basis for the explanation of the following measurements of heat transfer and friction characteristics in a baffled channel. Then, empirical correlations for average Nusselt numbers and friction factors are developed in terms of baffle and flow parameters. Finally, pumping power performance between the porous- and solid-type-baffled channels is analyzed to determine the effectiveness of the baffled channel. The work described here is believed to be one of the first fundamental studies of periodically porous-type-baffled channels in the open literature.

Experimental Apparatus

The flow system, as shown in Fig. 1, is operated in suction mode and oriented horizontally. Air is drawn into the settling chamber from the temperature-controlled laboratory room, traverses the bell-like channel entrance, flows through the baffled channel, a mixing chamber, and a flow meter, and then is exhausted by a 3-hp blower.

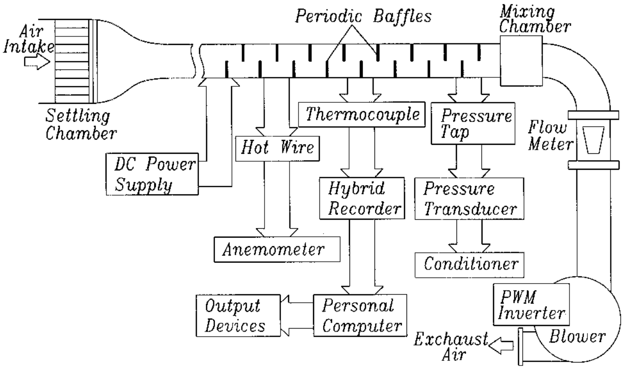

Fig. 1 Schematic drawing of flow system and experimental apparatus.

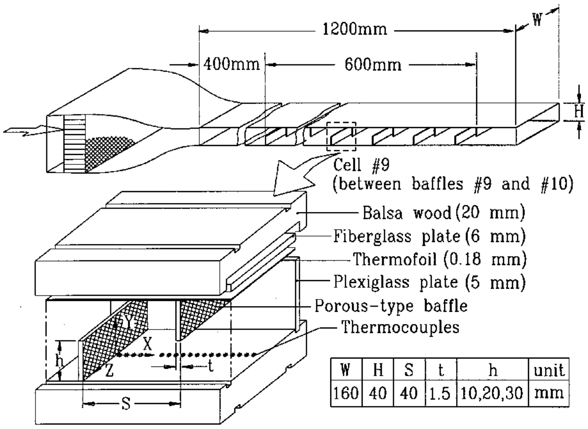

W	H	S	t	h	unit
160	40	40	1.5	10,20,30	mm

Fig. 2 Sketch of test section configuration and coordinate system.

The detail configuration of the test channel and the coordinate system are shown in Fig. 2 schematically. The test channel has a rectangular cross section of 40 by 160 mm (H by W), and a length of 1200 mm. The top and bottom horizontal walls of the test section are heat transfer surfaces, and the remaining two walls are thermally insulated. A 0.18-mm-thick stainless-steel thermofoil is adhered uniformly on the fiberglass board (6 mm in thickness), and is connected with a dc power supply for controllable electrically heating to the test section. To prevent conductive heat losses a piece of balsa wood 20 mm thick is adhered uniformly on the back side of the heated plate. Sixty porous-type baffles 1.5-mm (t) are transversely and staggeringly attached on the two heat transfer surfaces by using thermally conducting epoxy cement (electrically insulated). The first baffle is located 400 mm downstream of the channel inlet. The porous-type baffle is made of sintered bronze beads (85% Cu plus 15% Sn) with a mean diameter of 0.72 mm. This type of porous medium in sintered metals has been widely used in industrial applications such as heat exchangers, fluid filter, etc. The corresponding flow and thermophysical properties of this material are carefully measured and listed in Table 1. Note that the effective thermal conductivity is measured by an experimental apparatus produced by the Tokyo Meter Co., Ltd., model HVS-40-200-SD. By performing a number of one-dimensional conduction heat transfer experiments, the effective thermal conductivity could be found. The void fraction (or porosity) of the baffle is evaluated by $v_0 = (\boldsymbol{v}_t - v_s)/v_t$. The volume v_t is measured by its geometry, whereas v_s is determined by the volume of filling liquid.

From the flowfield measurements in the previous works,[3,4] it has been found that the hydraulic periodicity of the airflow was achieved in the region after the flow passed over four baffles. Moreover, the results obtained by Molki and Mostoufizadeh[11] showed that the thermal entrance length was about 1.4 times the channel hydraulic diameter (about after the third baffle-pair) for $h/H = 0.5$. Accordingly, in this work the temperature and flowfield measurements are done for the region

Table 1 Thermophysical properties of the solid- and porous-type baffles

Baffle type	v_O	ρ, kg/m^3	k_e, W/m K
Porous	0.42	4986	16.88
Solid	0	8600	26.68

between the 9th and 11th baffles (across two baffle cells, i.e., cells no. 9 and 10) to deduce the periodically fully developed heat transfer and fluid-flow data. In fact, the thermal periodicity has been verified using the present local Nusselt number distribution in cells no. 9 and 10, and there is only a 4% difference at the corresponding locations relative to the baffle. As shown in Fig. 2, 40 copper-constantan thermocouples (20 for the top wall and 20 for the bottom wall) are distributed along the spanwise centerline of the heated surfaces for wall temperature measurements. The junction beads (about 0.15 mm in diameter) of the thermocouples are carefully embedded into the channel walls, and then ground flat to ensure that they are flush with surfaces. Additionally, in the corresponding region, the channel midplane ($Z = 0$) is instrumented with thermocouple probes through the side wall to allow the airflow temperature measurements at 338 locations (26 by 13 for X by Y). The temperature signals are transferred to a hybrid recorder. All data are then sent to a PC-486 via GPIB interface. The preprocessing of the raw data are done in a built-in Basic program where the nondimensional parameters are calculated. As for flowfield measurements, the bottom heated plate is replaced by a Plexiglas® plate, and experiments are carried out under unheated conditions. A hot-wire anemometer (DISA) with a normal I-type probe is employed to measure the local velocity and turbulence intensity. The probe is mounted on a motor-driven linear translation stage (Klinger UT-100, 10 μm in resolution), and inserted from the bottom plate to traverse across the section to any desired location in the flow. The measurements of transverse mean velocity and turbulence intensity distributions are done at stations of $X/S = 0.2$, 0.5, and 0.8 across the channel midplane ($Z = 0$). To measure the fully developed static pressure differences of the baffled channel, two pressure taps are located at the bottom channel wall after the 7th and 11th baffles, respectively. The pressure signals from each pressure tape are transferred to a microdifferential transducer and subsequently amplified to a digital readout.

Data Reduction and Uncertainty

Centerline Local Heat Transfer Coefficients

The local convection heat transfer coefficient of the heated surface is presented in terms of the centerline Nu, which is defined as

$$Nu = Q_{\text{conv}} \cdot De/[A \cdot (T_w - T_b) \cdot k_f] \tag{1}$$

where

$$Q_{\text{conv}} = Q - Q_{\text{loss}}$$

Q_{conv} is calculated by subtracting Q_{loss} from Q. The electrical power generated from the thermofoil is determined from the measured thermofoil resistance and the current through the thermofoil on each surface. It is also checked by measuring voltage drop across each thermofoil. The effect of the temperature variation on the local thermofoil is calculated to be small and negligible. Thus, the thermofoil ensured a nearly uniform heat flux on each surface of the test channel. The heat loss can be estimated by the following equation:

$$Q_{\text{loss}} = Q_{\text{sc}} + Q_r + Q_{\text{ac}} \tag{2}$$

Q_{sc} is the conductive heat loss from the back sides of the heated plates (baffled walls) and the vertical adiabatic plates (smooth walls) to the environment, and is estimated to be less than 6 and 8%, respectively, for the range of Reynolds number tested. The radiative heat loss from the baffled surface ($\varepsilon = 0.09$) to its surroundings, Q_r, is evaluated by a diffuse gray surface network,[12] and is less than 0.5% of the total electrical power input. Q_{ac} is estimated to be less than 2% of the total electrical power input for a Reynolds number larger than 1×10^4. The total net heat transfer rate from the test channel to the cooling air is further checked with the cooling air enthalpy rise along the test channel. That is $Q_{\text{conv}} = G_{cp}(T_{bO} - T_{\text{in}})$. A comparison of Q_{conv} determined from the previous two methods shows only 5% in discrepancy, which confirms good energy conservation in the experiments. To place the results on a common basis the heat transfer area in Eq. (1) serves as the projected area of the corresponding baffleless wall. The Nusselt number thus obtained can reflect the conduction effect caused by the baffle (fin effect) as well as the enhanced turbulence effect by distorting velocity and temperature fields caused by the existence of baffle.

T_w used in Eq. (1) is the local wall temperature on the channel centerline (Fig. 2), which is read from the hybrid recorder directly. T_b is calculated from the equation

$$T_b = \frac{\int_0^H |U| T \, dY}{\int_0^H |U| \, dY} \tag{3}$$

where U and T are the local transverse (mean) velocity and temperature along the channel midplane ($Z = 0$), respectively. During this experiment, T_b is measured at three axial stations inside a baffle cell, i.e., $X/S = 0.2$, 0.5, and 0.8. At each axial station, T_b is represented by the value averaged over 13 measuring points from $Y/H = 0.05$ to 0.95. Then, at any other station the local bulk mean temperature of air is calculated by interpolation or extrapolation, and only 3% maximum deviation is found as compared with the measured data of Eq. (3). As the estimation by the method of Kline and McClintock[13] shows, the maximum uncertainty of the Nusselt number is less than 8.6% for a Reynolds number larger than 1×10^4.

Centerline Average Heat Transfer Coefficients

The centerline average Nusselt number for the periodically fully developed region is also calculated by Eq. (1). The only difference is the use of the average temperature difference $\bar{T}_w - \bar{T}_b$ instead of the local temperature difference $T_w - T_b$, where $\bar{T}_w$ is an average value of the 20 thermocouple readings at the top and bottom channel walls within a baffled cell, and $\bar{T}_b$ is represented by the average of the local bulk temperature at the three axial stations of $X/S = 0.2$, 0.5, and 0.8.

To reduce the influence of the Reynolds number, both the local and average Nusselt number of the present study are normalized by the Nusselt number for fully developed turbulent flow in smooth circular tubes correlated by Dittus and Boelter[14] as

$$Nu/\overline{Nu}_s = Nu/(0.023 \cdot Re^{0.8} \cdot Pr^{0.4}) \tag{4}$$

Friction Factors

The friction factor of the periodically fully developed flow is calculated from the pressure drop across the test channel and the bulk velocity of the air and expressed as

$$f = [-(\Delta P/\Delta X) \cdot De]/(\rho_a \cdot U_b^2/2) \tag{5}$$

where the pressure gradient $\Delta P/\Delta X$ is evaluated by taking the ratio of the pressure difference and the distance of two pressure taps. Note that based on the heating level of this study, it is experimentally determined that the friction factor with heating is only about 2% higher than that without heating. Therefore, the friction factor is based on the isothermal conditions (tests without heating). The maximum uncertainty of f is estimated to be less than 7.3% for a Reynolds number greater than 1×10^4 by the uncertainty estimation method of Kline and McClintock.[13]

The maximum uncertainties of other measured properties are as follows: U, ±2.4% and $\sqrt{u^2}$, ±8.2%.

Results and Discussion

Before the subsequent discussion, it is necessary to make a comparison of the present data with those in previous works to validate present experimental procedure and results. Because no data could be found to compare with the present work for porous-type-baffled results, the present data of fully developed heat transfer coefficients and friction factors are compared with those in the previous works for the smooth channel. As shown in Fig. 3, the average Nusselt number and friction factor for the present smooth channel wall is plotted as a function of Reynolds number. It is found from this figure that the maximum difference between the present data points and the values of friction factor predicted by a Blasius equation and by Rosen (cited by Rehsenow and Choi[15]) is only 6.2 and 8%, respectively. Another comparison given by this figure further reveals that the Nusselt numbers measured in this work coincide well with the empirical equation correlated by Dittus and Boelter,[14] with 4% in maximum deviation. The good agreement of the previous comparisons confirms adequate experimental procedures employed and reliable results obtained in the current work.

Flowfield Measurement

Figure 4 shows the flow-visualization results of the flow patterns around the solid- and porous-type baffles, which are measured by the smoke-wire technique. The smoke wires are placed vertically along the channel center on the axial stations of X/S = 0.2 and 0.5 for Figs. 4a and 4b, respectively. The flow is from left to right. This figure shows that flow patterns around the solid- and porous-type baffles are rather different. The flow reversal exists behind the solid-type baffle but is not present for the porous-type-baffled geometry. This indicates that the recirculating cell after the baffle disappears, as the solid-type baffle is replaced by the porous-type baffle on the channel wall. Physically, the flow over the solid-type baffles could be characterized as a turbulent shear flow, which is introduced from the baffle tip and drives a large recirculation bubble downstream of the left baffle with flow downward near the bottom wall and the right baffle.[4] The zigzag-motion mean flow across a number of staggered baffles in the channel will impinge on the top and bottom channel walls by turns. As for flow over the porous-type baffles, a part of fluid passes through the porous medium and the remainder goes around the baffles. It is further seen that the flow structures between the lower- and upper-half parts of the porous-type-baffled channel are significantly different. At the lower-half part, the small turbulence eddies are observed behind the porous-type baffle, which results from the multi-mixing-layer interaction as the fluid passes through the porous-type baffle. However, this phenomenon could not be found in the upper-half part of the porous-type-baffled channel. This will be reflected by the higher turbulence intensity and will be shown later.

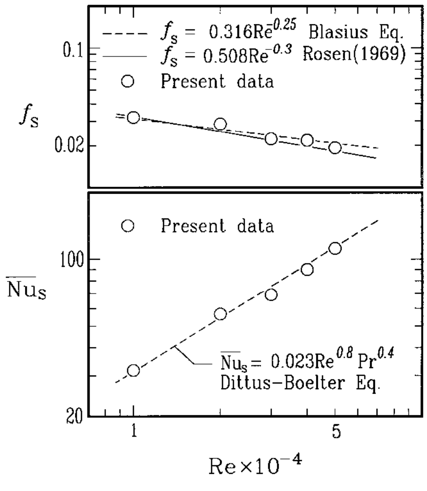

Fig. 3 Fully developed average Nusselt number and friction factor for the smooth channel.

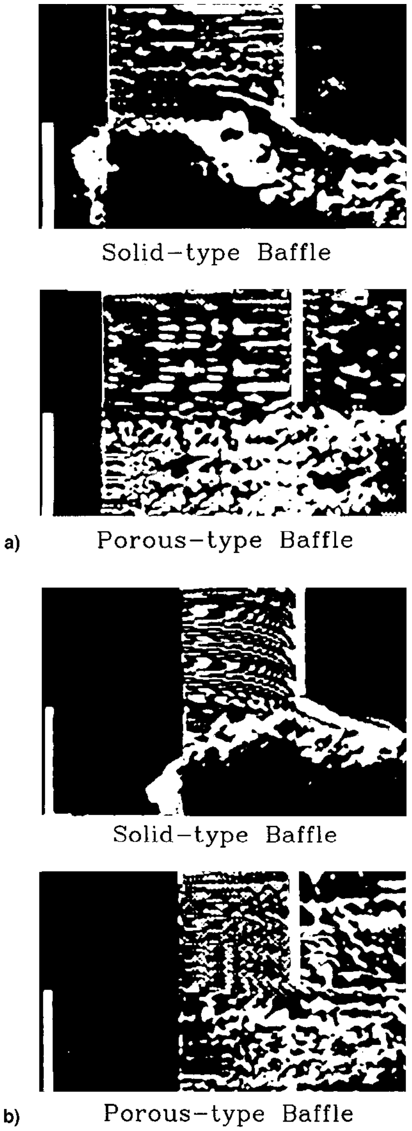

Fig. 4 Flow patterns of the flow over the solid-type and porous-type baffles, smoke wire is placed at stations of a) X/S = 0.2, and Z = 0, Re = 1 × 10^4 and b) X/S = 0.5, and Z = 0, Re = 1 × 10^4.

The measured streamwise mean-velocity and turbulent-intensity profiles at the axial stations of X/S = 0.2 and 0.5 for flow over the solid- and porous-type baffles are shown in Fig. 5 for h/H = 0.5 and Re = 3 × 10^4. The open and solid symbols are pertinent to the solid- and porous-type symbols, respectively. Note that the flow direction, particularly in the flow reversal, cannot be detected by the present technique (I-type hot wire). It is therefore employing the flow-visualization results shown previously to assist the presentation of mean-flow results. As given in Fig. 5a, there is no data presented on the broader-dashed lines between two open symbols (solid-type baffle) because of the uncertainties of flow direction. The flow

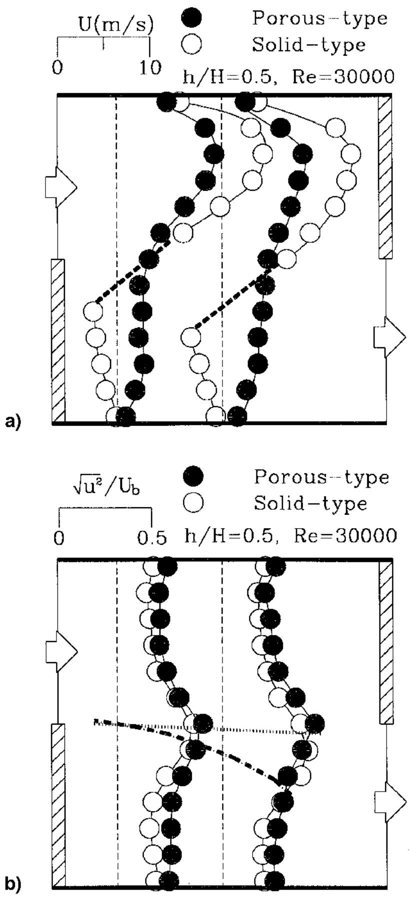

Fig. 5 Streamwise a) velocity and b) turbulent intensity profiles along the channel midplane ($Z = 0$) at stations of $X/S = 0.2$ and 0.5.

patterns around solid-type baffles have been described before, and are not elaborated on here. As for the porous-type baffles, the flow decelerates before encountering the porous-type baffles (upper-half part), and accelerates as it goes through the full opening between the baffles and the channel walls (lower-half part). The progressing flow accelerates and decelerates alternatively so that, in turn, it promotes a large shear turbulence because of the mixing-layer interaction. The measurements of the root-mean squares of the velocity fluctuation in the streamwise direction are presented in Fig. 5b. Globally, the streamwise turbulence intensity profiles for the porous-type baffles is slightly higher than those for the solid-type baffles. It is further seen from this figure that the peak value of $\sqrt{u^2}$ moves from $Y/H = 0.5$ slightly downward to $Y/H = 0.4$ as the flow proceeds forward from $X/S = 0.2$–0.5. This slight shift corresponds to the convergence of the dividing streamline (dashed–dotted line) toward the bottom wall. However, this phenomenon could not be observed for the porous-type baffle, in which the peak of $\sqrt{u^2}$ almost keeps $Y/H = 0.5$ (dotted line) as the axial stations are varied.

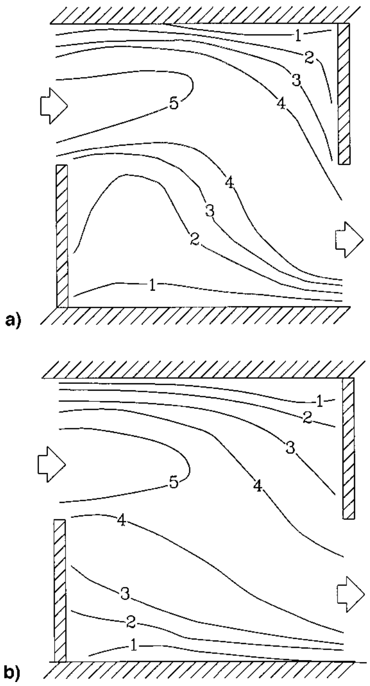

Fig. 6 Isothermal contours for the a) solid- and b) porous-type-baffled channels along the channel midplane ($Z = 0$), $Re = 3 \times 10^4$ (1:68, 2:62, 3:56, 4:50, 5:44, unit: °C).

Isotherm Patterns

The isothermal contours of the thermal field around the solid- and porous-type baffles are shown in Figs. 6a and 6b for $Re = 3 \times 10^4$ and $h/H = 0.5$, respectively. The air flows from the upper left to the lower right of the cell formed between baffles. Several evident discrepancies of the isotherm patterns between the solid- and porous-type baffles could be observed from these two graphs. First, the temperature distributions behind the upstream solid-type baffle are significantly higher than those in the corresponding region of the porous-type baffle. As for flow over the solid-type baffle, the fluid turning from the upstream bottom channel wall into the contraction introduces a strong shear layer from the baffle tip approaching the bottom wall, which forms a large recirculation bubble behind the baffle. The curved shear layer acts as an adiabatic wall, which prevents the heat transfer from the recirculation region to the main flow via convection.[16] Consequently, the related higher temperature distributions are found in this region. It is further seen from this figure that in the recirculating cell the temperature distribution is rather uniform. As for the flow over the porous-type baffles, airflow partly passes through the baffle and directly impinges the recirculation cell, and hence breaks up the recirculating bubble. Therefore, the temperature distribution in this region ($0 < X/S < 0.5$, and $0 < Y/h < 0.5$) is significantly lower than that for the solid-type baffle. Clearly, the transport phenomena in this region have been greatly improved when the solid-type baffles are replaced by the porous-type baffles on the channel wall. Additional outcomes will be discussed later for the comparison of local heat transfer distributions along the baffled wall. Another notable feature given in Fig. 6 shows that the upward tongue-shaped isotherm is found at the entrance of the baffle cell (upper-left corner) for the solid-type baffle. But this is not found in the porous-type baffle. This fact is easily verified by comparing U near the top channel wall as shown in Fig. 5a. In fact, this significant washing action on the top wall for the solid-type baffle because of highly deflected flow is further reflected on the thinner thermal boundary layer (or higher temperature gradient) near the top channel wall.

Local Nusselt Number Distributions Along the Channel Midplane

Typical results showing the distributions of the local Nusselt number ratio along the porous- and solid-type-baffled walls are presented at the same baffle height ($h/H = 0.5$) and flow Reynolds number ($Re = 3 \times 10^4$) in Fig. 7. Along the top wall of the solid-type-baffled channel, the local Nusselt number ratio distributions slightly increase to a local maximum at about $X/S = 0.25$ because of the impingement of the flow on the channel wall. Then, it decreases rapidly because of the development of the thermal boundary layer (Fig. 5a). Finally, the value is slightly increased to another local maximum before encountering the right baffle, which is caused by an abundant

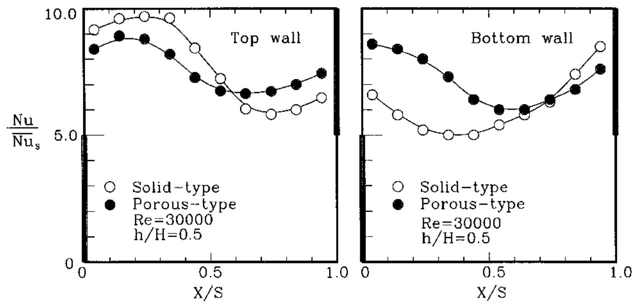

Fig. 7 Local centerline Nusselt number distributions along the solid- and porous-type-baffled walls.

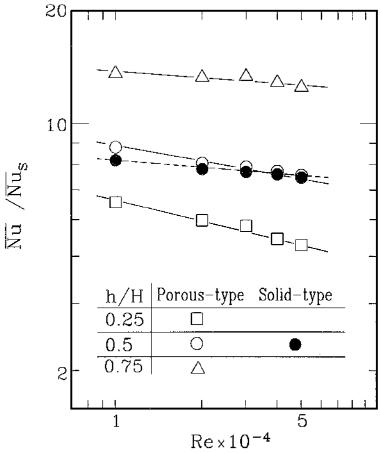

Fig. 8 Reynolds number dependence of centerline-averaged Nusselt number for the baffled walls.

energy conducted through the top wall (base) into the baffle. As for the porous-type-baffled wall, similar distributions of the local Nusselt number ratio are observed. However, the values of the first and the second peaks are, respectively, lower and higher than the corresponding values of the solid-type baffle. The former is because of the lower augmented forced convection by flow acceleration between the baffle top and channel wall for the porous-type baffle (Fig. 5a). This fact is also readily confirmed by the thicker thermal boundary layer accompanied by the porous-type-baffled channel in this region (Fig. 6). The latter is because a larger amount of heat could be conducted into the porous-type baffle through the baffle base as compared with that from the solid-type baffle. Note that effective conductivity of the porous-type baffle is that, although lower than that of the solid-type baffle (Table 1), the heat transfer surface area of the porous-type baffle is significantly larger than that of the solid-type baffle. Therefore, a larger fraction of heat transferred by the porous-type baffle is very reasonable. It is concluded from the previous results that the conductive effect (fin effect) and the force-convection effect for the porous-type baffle are, respectively, better and worse than those for the solid-type baffle.

On the bottom channel wall the local Nusselt number ratio of the solid-type baffle starts a local maximum just downstream of the baffle, decreases sharply to a local minimum, and then increases to another local maximum before the flow enters the next baffle cell. Also, the first peak results from the conductive heat routed through the bottom wall into the baffle. The significantly lower heat transfer coefficient in the region of $X/S = 0.1$–0.5 is because of the recirculation bubble presented in this region. Another local maximum near $X/S = 1.0$ is because of the tendency of flow impingement on the bottom wall. The same phenomenon was obtained by the calculation of Kelkar and Patankar[8] at $h/H = 0.5$, and $S/H = 1.0$ for laminar flow ($Re = 5 \times 10^2$). As for the porous-type baffle, a similar but smoother trend is observed.

Table 2 Coefficients for Eqs. (6) and (7)

Baffle type	h/H	c_1	c_2	d_1	d_2
Porous	0.25	28.27	−0.175	14.23	−0.131
	0.50	26.55	−0.118	22.75	0
	0.75	62.61	−0.098	49.88	0
Solid	0.50	19.35	−0.092	31.64	0

Fully Developed Centerline Heat Transfer Coefficients

The Reynolds number dependence of the centerline-averaged Nusselt number ratio for the solid- and porous-type-baffled walls is displayed in Fig. 8. The symbols represent the actual experiments and the solid lines passing through these symbols are curve-fitting results. The equations of these lines can be expressed as

$$\overline{Nu}/\overline{Nu}_s = c_1 Re^{c_2} \tag{6}$$

where the values of the coefficients c_1 and c_2 are listed in Table 2 for various baffle heights and baffle types. The maximum deviation between Eq. (6) and the experimental data shown in Fig. 8 is less than 5%. It can be seen from this figure that both the porous- and solid-type-baffled walls give rise to substantial enhancement relative to the smooth channel. The extent of the enhancement in Nusselt number is larger at lower Reynolds number. As can be seen from this figure or the previous equations, the average heat transfer ratio decreases with increasing Reynolds number for both the solid- and porous-type-baffled walls. It is further found that at the same baffle height $h/H = 0.5$ the level of heat transfer augmentation is nearly the same for the solid- and porous-type baffles, the only difference being the Reynolds number dependence. The Reynolds number dependence on the average Nusselt number ratio for the porous-type baffles ($Re^{0.682}$) is slightly lower than that for the solid-type baffles ($Re^{0.708}$); and both are lower than that given in Eq. (4) for the smooth wall ($Re^{0.8}$). The explanation is that in the porous-type-baffled wall part of the mean-flow energy (this can be regarded as the flow Reynolds number effect) used for convection heat transfer has transferred into turbulence kinetic energy, which subsequently enhances the heat transfer rate through enhanced turbulent transport (Fig. 5b). As for the effect of baffle height, the Nusselt number ratio increases as expected with increasing baffle height because of the augmentation of the flow acceleration that is caused by the increase of the cross-sectional blockage of the channel. A similar trend was found for the channel with solid-type baffles.[5]

It is concluded from the previous discussion that there are three effects present when the solid-type baffles are replaced by the porous-type baffles on the channel wall. One is the effect of reducing the effective thermal conductivity of the baffle (Table 1), which is owing to the existence of air within the porous-type baffle. The second is the effect of the increase of heat transfer surface area because of flow through the porous-type baffles. The third effect is to change the flow transport phenomena (Figs. 4 and 5). Obviously, the combination of the previously mentioned effects is competing with each other when the porous-type baffles with $v_0 = 0.42$ are applied on the channel wall instead of the solid-type baffles; and hence an insignificant change in the overall heat transfer coefficient is reached. It should be noted that the previous trend is valid for the baffle porosity being 0.42 and may not be true if the porosity is varied, especially for the very high baffle porosity. Nevertheless, the distribution of the local heat transfer coefficient along the channel wall, which has been addressed in the previous section, is highly influenced by the previously mentioned effects.

Pressure Drop

The dependence of friction factor on the Reynolds number for the solid- and porous-type-baffled geometries is shown in

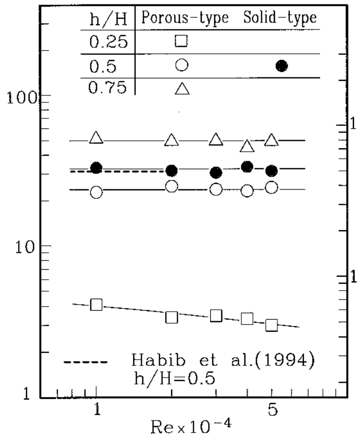

Fig. 9 Fully developed friction factor vs Reynolds number for the baffled channels.

Fig. 9. The baffle spacing is fixed at $S/H = 1$. The solid and open symbols in this figure represent the results of the solid- and porous-type baffles, respectively. K [defined as $2\Delta P/(\rho\cdot U_b^2)$], often used in pipe fittings to represent the pressure losses, is also provided in this figure. For the higher baffles, $h/H = 0.5$, and 0.75, the friction factor is nearly independent on the Reynolds number and stays almost at a constant value as the Reynolds number varies; whereas with $h/H = 0.25$, the data show a tendency to decrease with an increase in Reynolds number. This is mainly because of the difference in the relative contribution of the profile and viscous drags in channels with different heights of baffles.[17] A similar conclusion was made by Berner et al.[4] for the solid-type-baffled channel. A comparison is also made in this figure between the present solid-type-baffled results and those of the previous work,[5] and a good agreement is achieved. It is further seen that the porous-type-baffled channel has a considerably smaller friction factor as compared with that for the solid-type-baffled geometry, typically only about 71% for $h/H = 0.5$, and $S/H = 1.0$. This is very reasonable because the less cross-sectional blockage is accompanied by the porous-type baffles, which largely reduces the form drag of a baffled channel. As for the effect of baffle height, the friction factor increases with increasing h/H for a fixing baffle spacing and a given Reynolds number. The data presented in Fig. 9 could be correlated as the following equations:

$$f = d_1 Re^{d_2} \tag{7}$$

where the coefficients d_1 and d_2 are listed in Table 2 for various baffle types and heights. The maximum deviation between Eq. (7) and the experimental data is only 6%.

Pumping Power Performance

There is a broad variety of constraints that may be utilized[18,19] in comparing the performance of the baffled and smooth heat transfer passages. In this paper, performance comparisons between two types of baffled channels are made for two sets of constraints that are widely employed, namely, the same airflow rate and the same pumping power. The comparison of heat transfer coefficients for the same airflow rate constraint has already been made in Fig. 8. Attention is now turned to the same pumping power constraint. With baffles applied on the channel wall, the pressure drop should be increased. Therefore, the mass flow rate must be reduced to keep the fluid pumping power constant, which will lead to a reduction in average Nusselt number. Sometimes this reduction can be overcome by heat transfer enhancement given by baffles. To implement this case, the pumping power (PP) required to drive a flow rate G through ΔP should be noted as

$$\mathrm{PP} = (G/\rho)\cdot\Delta P \tag{8}$$

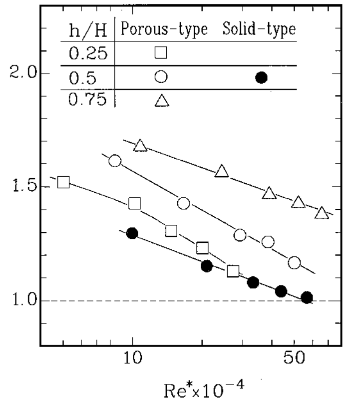

Fig. 10 Comparison of thermal performance between solid- and porous-type-baffled channels under constant-pumping-power conditions.

For a baffled channel and a smooth channel that have equal hydraulic diameters and lengths, it is readily shown that the constraint of equal blowing power can be reduced to

$$(f\cdot Re^3)_{\text{baffled channel}} = (f\cdot Re^3)_{\text{smooth channel}} \tag{9}$$

Thus, in Fig. 10 the performance shown by the ratio of $\overline{Nu_p}/\overline{Nu_s^*}$ is plotted against $(f/f_s)^{1/3}\cdot Re$, where $\overline{Nu_s^*}$ is the average Nusselt number for a smooth channel with the flow rate at which the pumping power is the same as that obtained in the baffled channel.[20] From this figure it is seen that the channel with porous-type baffles performs better than the solid-type-baffled geometry. This is because a moderate heat transfer enhancement and a dramatically lower pressure drop are followed by the porous-type baffle (Figs. 8 and 9). Figure 10 shows that the improvement in the Nusselt number ratio decreases with increasing Reynolds number. That is, at lower Reynolds number, both the porous- and solid-type-baffled geometries could give a higher thermal performance than those at higher Reynolds number.

Summary and Conclusions

An experimental study has been presented for turbulent flow and heat transfer in a rectangular channel with segmented porous-type baffles that are staggeringly arranged on the top and bottom of the channel. The experiments are carried out for a fixed baffle porosity ($v_0 = 0.42$) and spacing ($S/H = 1.0$), and different values of Reynolds number ($1 \times 10^4 \leq Re \leq 5 \times 10^4$) and baffle heights ($h/H = 0.25, 0.5$, and 0.75). Conclusions reached from the experiments are as follows:

1) Replacing the solid-type baffle by the porous-type baffle in a channel has an effect of changing the transport phenomena around the baffles. The recirculation bubble that existed behind the solid-type baffle disappears in the corresponding region of the porous-type baffle.

2) For porosity of the baffle being 0.42, the local heat transfer coefficient distributions along the channel centerline are significantly different to those along solid-type-baffled walls. However, the discrepancy in the average heat transfer coefficient is insignificant between the porous- and solid-type-baffled walls if the baffle height ($h/H = 0.5$) and spacing ($S/H = 1.0$) are fixed.

3) Relative to the solid-type-baffled channel, the porous-type-baffled channel has a dramatically lower friction factor (or loss coefficient) because of less channel blockage, typically only about 71% of the friction factor at $h/H = 0.5$ and $S/H = 1.0$.

4) Thermal performance evaluation reveals that the porous-type-baffled channel could perform better than the solid-type-baffled channel at the constant power constraint.

5) Correlations of the average Nusselt number and friction factor are developed in terms of Reynolds number for both the porous- and solid-type-baffled channels.

Acknowledgment

This work was sponsored by the National Science Council of the Republic of China under Contract NSC 85-2212-E-216-003.

References

[1] Gunter, A. Y., Sennstrom, H. R., and Kopp, S., "A Study of Flow Patterns in Baffled Heat Exchangers," American Society of Mechanical Engineers, Paper 47-A-103, Jan. 1947.

[2] Gay, B., Mackley, N. V., and Jenkins, J. D., "Heat Transfer in Baffled Cylindrical Shell-and-Tube Exchangers — An Electrochemical Transfer Modeling Technique," *International Journal of Heat and Mass Transfer*, Vol. 19, No. 8, 1976, pp. 995–1002.

[3] Founti, M. A., and Whitelaw, J. H., "ShellSide Flow in a Model Disc and Doughnut Heat Exchanger," Mechanical Engineering Dept., Imperial College, TR FS/81/37, London, 1981.

[4] Berner, C., Durst, F., and McEligot, D. M., "Flow Around Baffles," *Journal of Heat Transfer*, Vol. 106, Nov. 1984, pp. 743–749.

[5] Habib, M. A., Mobarak, A. M., Sallak, M. A., Hadi Abdel, E. A., and Affify, R. I., "Experimental Investigations of Heat Transfer and Flow over Baffles of Different Heights," *Journal of Heat Transfer*, Vol. 116, May 1994, pp. 363–368.

[6] Rowley, G. J., and Patankar, S. V., "Analysis of Laminar Flow and Heat Transfer in Tubes with Internal Circumferential Fins," *International Journal of Heat and Mass Transfer*, Vol. 27, No. 4, 1984, pp. 553–560.

[7] Webb, B. W., and Ramadhyani, S., "Conjugate Heat Transfer in a Channel with Staggered Ribs," *International Journal of Heat and Mass Transfer*, Vol. 278, No. 9, 1985, pp. 1679–1687.

[8] Kelkar, K. M., and Patankar, S. V., "Numerical Prediction of Flow and Heat Transfer in a Parallel Plate Channel with Staggered Fins," *Journal of Heat Transfer*, Vol. 109, No. 1, 1987, pp. 25–30.

[9] Habib, M. A., Attya, A. E., and McEligot, D. M., "Calculation of Turbulent Flow and Heat Transfer in Channels with Streamwise-Periodic Flow," *Journal of Turbomachinery*, Vol. 110, April 1988, pp. 405–411.

[10] Lopez, J. R., Anand, N. K., and Fletcher, L. S., "Heat Transfer in a Three-Dimensional Channel with Baffles," *Numerical Heat Transfer, Part A: Applications*, Vol. 30, No. 2, 1996, pp. 189–205.

[11] Molki, M., and Mostoufizadeh, A. R., "Turbulent Heat Transfer in Rectangular Ducts with Repeated-Baffle Blockages," *International Journal of Heat and Mass Transfer*, Vol. 32, No. 8, 1989, pp. 1491–1499.

[12] Siegel, R., and Howell, J. R., *Thermal Radiation Heat Transfer*, 2nd ed., McGraw–Hill, New York, 1981.

[13] Kline, S. J., and McClintock, F. A., "Describing Uncertainties on Single-Sample Experiments," *Mechanical Engineering*, Vol. 57, Jan. 1953, pp. 3–8.

[14] Dittus, F. W., and Boelter, L. M. K., *Publications in Engineering*, Vol. 2, Univ. of California, Berkeley, CA, 1930, p. 443.

[15] Rohsenow, W. M., and Choi, H. Y., *Heat Mass and Momentum Transfer*, Prentice–Hall, Englewood Cliffs, NJ, 1969.

[16] Liou, T. M., and Hwang, J. J., "Turbulent Heat Transfer and Friction in Periodic Fully Developed Flows," *Journal of Heat Transfer*, Vol. 114, Feb. 1992, pp. 56–64.

[17] Perry, A. E., Schofield, W. H., and Joubert, P. N., "Rough Wall Turbulent Boundary Layers," *Journal of Fluid Mechanics*, Vol. 37, 1969, pp. 383–413.

[18] Bergles, A. E., "Survey and Evaluation of Techniques to Augment Convective Heat and Mass Transfer," *Progress in Heat and Mass Transfer*, Pergamon, Oxford, England, UK, Vol. 1, 1969, pp. 324–331.

[19] Webb, R. L., "Toward a Common Understanding of the Performance and Selection of Roughness for Forced Convection," *Studies in Heat Transfer*, Hemisphere, Washington, DC, 1979, pp. 257–272.

[20] Hwang, J. J., and Liou, T. M., "Heat Transfer in a Rectangular Channel with Perforated Turbulence Promoters Using Holographic Interferometry Measurement," *International Journal of Heat and Mass Transfer*, Vol. 38, No. 17, 1995, pp. 3197–3207.